

See discussions, stats, and author profiles for this publication at: <https://www.researchgate.net/publication/261063803>

Crystallization-Driven Self-Assembly of Block Copolymers with a Short Crystallizable Core-Forming Segment: Controlling Micelle Morphology through the Influence of Molar Mass and So...

ARTICLE *in* MACROMOLECULES · MARCH 2014

Impact Factor: 5.8 · DOI: 10.1021/ma402429d

CITATIONS

17

READS

61

4 AUTHORS, INCLUDING:



Ming-Siao Hsiao

Air Force Research Laboratory, WPAFB

22 PUBLICATIONS 307 CITATIONS

[SEE PROFILE](#)

Crystallization-Driven Self-Assembly of Block Copolymers with a Short Crystallizable Core-Forming Segment: Controlling Micelle Morphology through the Influence of Molar Mass and Solvent Selectivity

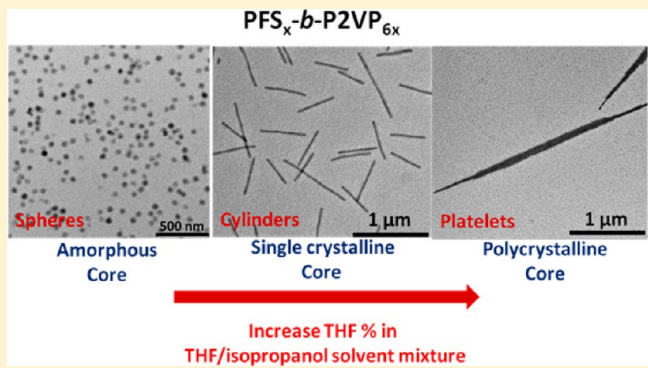
Ming-Siao Hsiao,^{†,§} Siti Fairus M. Yusoff,^{†,||} Mitchell A. Winnik,^{*,‡} and Ian Manners^{*,†}

[†]School of Chemistry, University of Bristol, Bristol BS8 1TS, U.K.

[‡]Department of Chemistry, University of Toronto, Toronto, Ontario, Canada M5S 3H6

Supporting Information

ABSTRACT: Three well-defined asymmetric crystalline-coil poly(ferrocenyldimethylsilane-*b*-2-vinylpyridine) (PFS_x -*b*-P2VP) diblock copolymers (PFS_{44} -*b*-P2VP₂₆₄, PFS_{75} -*b*-P2VP₄₅₄, and PFS_{102} -*b*-P2VP₆₂₅) with similar block ratios ($r = N_{\text{P2VP}}/N_{\text{PFS}} = \text{ca. } 6.0 \pm 0.1$) but different overall molar masses ($M_n = 38\,700$, $65\,800$, and $90\,400 \text{ g mol}^{-1}$) were synthesized by sequential anionic polymerization, and their solution self-assembly behavior was explored as a function of (i) molar mass and (ii) the ratio of common to selective solvent. When self-assembly was performed in isopropanol (i-PrOH), a selective solvent for P2VP, a decrease in the rate of the crystallization-driven transition from the initially formed spheres (with amorphous PFS cores) into cylinders (with crystalline cores) was detected with an increase in molecular weight. This trend can be explained by a decrease in the rate of crystallization for the PFS core-forming block as the chain length increased. In contrast, when a mixture of i-PrOH with increasing amounts of THF, a common solvent for both blocks, was used, spheres, cylinders, and also narrow lenticular platelets consisting of crystallized PFS lamellae sandwiched by two glassy coronal P2VP layers were formed from the same PFS_x -*b*-P2VP_{6x} sample. The most likely explanation involves the plasticization of the PFS core-forming block which facilitates crystallization, possibly complemented by contraction of the coils of the P2VP coronal block which otherwise limit the lateral growth of the crystalline PFS core as THF is a poorer solvent for P2VP than i-PrOH. Selected area electron diffraction studies indicated that the PFS cores of the spherical micelles were amorphous but were consistent with those of the cylindrical micelles existing in a state approximating to that of a monoclinic PFS single crystal. In contrast, in the platelets formed in THF/i-PrOH, the PFS cores were found to be polycrystalline. The formation of narrow lenticular polycrystalline platelets rather than a regular, rectangular single crystalline morphology was attributed to a poisoning effect whereby the interference of the long P2VP coronal blocks in the growth of a rectangular PFS single crystalline core introduces defects at the crystal growth fronts.



INTRODUCTION

The self-assembly of block copolymers has attracted growing attention as a result of their ability to form hierarchical ordered structures in either the solid state or solution that possess a wide variety of potential applications in nanoscience and nanomedicine.^{1–21} A variety of morphologies can be generated in thin films or the bulk state by controlling the polymer–polymer interaction parameter χ , volume fraction, and molecular weight of the block copolymer. In addition, when diblock copolymers are self-assembled in a selective solvent, a wide range of core–shell micelle morphologies including disks, cylinders, vesicles, and more complex structures have been reported. The resulting block copolymer micelles have attracted attention due to their potential utility as etch resists in nanolithography, for composite reinforcement, and as templates for biomedical applications such as drug delivery.^{2,4,6,9,12–16}

Whereas early work focused mainly on spherical micelles, in pioneering work by Eisenberg and co-workers, a broad spectrum of morphologies including cylinders, vesicles, network micelles were observed for crew-cut diblock copolymers such as poly(styrene-*b*-acrylic acid) in aqueous solution.^{22–25} Moreover, the stability of the various morphologies could be explained by the interplay of the electrostatic and steric interactions of the corona-forming blocks, the surface tension between the core-forming block and the solvent, and the stretching of the core-forming block. Hence, the micellar morphologies could be controlled by adjusting the parameters such as the sample composition, concentration, temperature, and solvent polarity.¹²

Received: November 26, 2013

Revised: February 25, 2014

Published: March 21, 2014

Until recently, the vast majority of studies of block copolymer self-assembly in solution focused on materials in which the core-forming block is amorphous. Lotz and Keller et al. first reported the influence of crystallization on the micelle morphologies in the mid-1960s in their studies of poly(styrene-*b*-ethylene oxide) (PS-*b*-PEO) in PS selective solvents such as ethylbenzene and xylene.^{26–28} These studies showed that the solvent is a selective solvent for PS but a theta or poor solvent for the crystallizable core-forming PEO block; thin square-shaped lamellar platelets are formed. These PS-*b*-PEO lamellar structures, which have since been further studied in much detail by several groups,^{29–32} consist of the PEO layer in a single crystalline state covered by two glassy PS layers. In 2000, as part of our studies of the solution self-assembly of metal-containing block copolymers with a core-forming polyferrocenyldimethylsilane (PFS) metalloblock,³³ we showed that core crystallization can lead to the preferred formation of either cylindrical micelles or platelet nanostructures depending on the ratio of crystallizable core to amorphous corona-forming block.^{34,35} Moreover, we found that the addition of further block copolymer unimers to pre-existing crystalline cylindrical seeds can lead to “living self-assembly” whereby the structures undergo controlled elongation by an epitaxial growth process.³⁶ This allows the formation of a variety of novel structures such as cylinders that are monodisperse in length, block comicelles with segmented corona and/or core structures, and novel morphologies such as scarf micelles.^{36–38}

Recently, studies of the solution self-assembly of crystalline-coil block copolymers have been extended to other materials^{37,39–67} including poly(ferrocenyldiethyldimethylsilane)⁶⁵ and poly(ferrocenyldimethylgermane)-based³⁷ diblock copolymers, poly(acrylonitrile-*b*-styrene) (PAN-*b*-PS),³⁹ poly(acrylonitrile-*b*-methyl methacrylate) (PAN-*b*-PMMA),³⁹ poly(caprolactone-*b*-ethylene oxide) (PCL-*b*-PEO),⁴⁰ poly(lactide),^{41–43} polythiophene,^{44–48} and polyethylene-containing diblock copolymers,^{49,50} and also triblock copolymers with crystallizable central blocks such as poly(styrene-*b*-ethylene-*b*-methyl methacrylate).^{51,52} Furthermore, morphology changes have been induced for micelles in the cases of crystalline-coil diblock copolymers such as PCL-*b*-PEO, poly(*N,N*-dimethylacrylamide-*b*-polyethylene), and poly(butadiene-*b*-ethylene oxide) (PB-*b*-PEO), etc.^{53–59} This has been achieved by adjusting the crystallization temperature,^{49,53–55} micelle concentration,⁵⁷ the amount of an inorganic salt,⁵⁸ and the solvent selectivity.^{54,59} Thus, crystallization of a core-forming block is emerging as a promising method for morphology control and the preparation of well-defined and potentially functional hierarchical architectures.^{41–67}

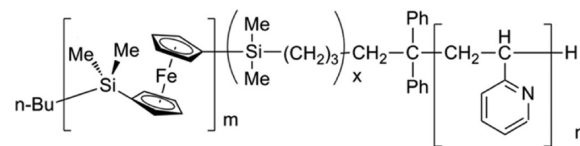
Poly(ferrocenyldimethylsilane-*b*-2-vinylpyridine) diblock copolymer (PFS-*b*-P2VP) has served as one of the most useful systems for probing the crystallization-driven self-assembly of diblock copolymers in solution.^{68–73} When the samples had a short PFS core-forming block ($N_{\text{PFS}} = 22$ or 23 and block ratio $r = N_{\text{P2VP}}/N_{\text{PFS}} = 7$ and 10),^{68,70} spherical micelles with a amorphous PFS core were formed in methanol, while a micellar sphere-to-cylinder transition driven by the crystallization of the PFS metalloblock occurred in both ethanol and isopropanol (*i*-PrOH) at room temperature.⁷⁰ The transition from spheres to cylinders was slower for the PFS-*b*-P2VP samples with a longer P2VP corona-forming block in ethanol (several minutes for $r = 7$ versus several weeks for $r = 10$).^{68,70} In contrast, we recently have identified a micellar sphere-to-platelet transition in THF/*i*-PrOH solvent mixtures at room temperature for PFS-*b*-P2VP samples with a short P2VP block ($r = 1$ and 0.2).⁷²

In this paper we describe detailed studies of the solution self-assembly of three $\text{PFS}_x\text{-}b\text{-P2VP}_{6x}$ samples with very similar block ratios ($r = N_{\text{P2VP}}/N_{\text{PFS}} = \text{ca. } 6.0$) but different molar masses. This has allowed us to probe the influence of molar mass on the micellar sphere-to-cylinder transitions for the three diblock copolymers in isopropanol. In addition, we have explored the influence of the ratio of the common solvent to selective solvent on micelle morphologies. The morphologies and the amorphous or crystalline nature of the micelle cores were confirmed utilizing various techniques including transmission electron microscopy (TEM), selected area electron diffraction (SAED), dynamic light scattering (DLS), and atomic force microscopy (AFM). Finally, possible mechanisms that account for the formation of the observed micellar structures are discussed.

RESULTS

1. Synthesis and Characterization of $\text{PFS}_x\text{-}b\text{-P2VP}_{6x}$ Diblock Copolymers. Three well-defined $\text{PFS}_x\text{-}b\text{-P2VP}_{6x}$ diblock copolymers having similar block ratio ($r = N_{\text{P2VP}}/N_{\text{PFS}} = \text{ca. } 6.0$) but different molecular weight were synthesized by multistage living anionic polymerization, and a detailed synthesis procedure was reported in previous works.^{68,74} The molecular structure of these three $\text{PFS}_x\text{-}b\text{-P2VP}_{6x}$ diblock copolymers is shown in Scheme 1. The polydispersities (PDIs) of the resulting

Scheme 1. Molecular Structure of the PFS-*b*-P2VP ($m:n = 1:6$) Diblock Copolymer ($x = 1–3$)



samples were determined using GPC (Figure S1), and ^1H NMR integration results (Figures S2–S4) were used to determine the block ratios and overall molecular weights (see SI for details). Characterization data for three $\text{PFS}_x\text{-}b\text{-P2VP}_{6x}$ samples are summarized in Table 1.

Table 1. Characterization Data for Three $\text{PFS}_x\text{-}b\text{-P2VP}_{6x}$ Samples

$\text{PFS}_m\text{-}b\text{-P2VP}_n$	$M_n^{\text{PFS}}\text{a}$ (g/mol)	$M_n^{\text{PFS-}b\text{-P2VP}}\text{c}$ (g/mol)	$N^{\text{PFS}}/N^{\text{P2VP}}\text{b}$	PDI ^a
$\text{PFS}_{44}\text{-}b\text{-P2VP}_{264}$	10 700	38 700	1:6.0	1.12
$\text{PFS}_{75}\text{-}b\text{-P2VP}_{454}$	18 100	65 800	1:6.0	1.12
$\text{PFS}_{102}\text{-}b\text{-P2VP}_{625}$	24 800	90 400	1:6.1	1.14

^aDetermined from triple detection GPC measurements with THF as the eluent. ^bFrom ^1H NMR signal integration for the two each blocks.

^cFrom the value of M_n^{PFS} and the block ratio.

2. Influence of Molecular Weight on the Micellar Sphere-to-Cylinder Transition. The micelle morphologies of three different $\text{PFS}_x\text{-}b\text{-P2VP}_{6x}$ diblock copolymers formed in pure isopropanol (*i*-PrOH) were studied at room temperature after they had first been gently sonicated at 27 °C in the solvent for 5 min to dissolve the material and form a clear solution (concentration = 0.16 g/L) followed by (i) a further period of 12 h at 27 °C or (ii) after heating at 64 °C for 1 h and cooling to ambient conditions. The temperatures were chosen to be close to

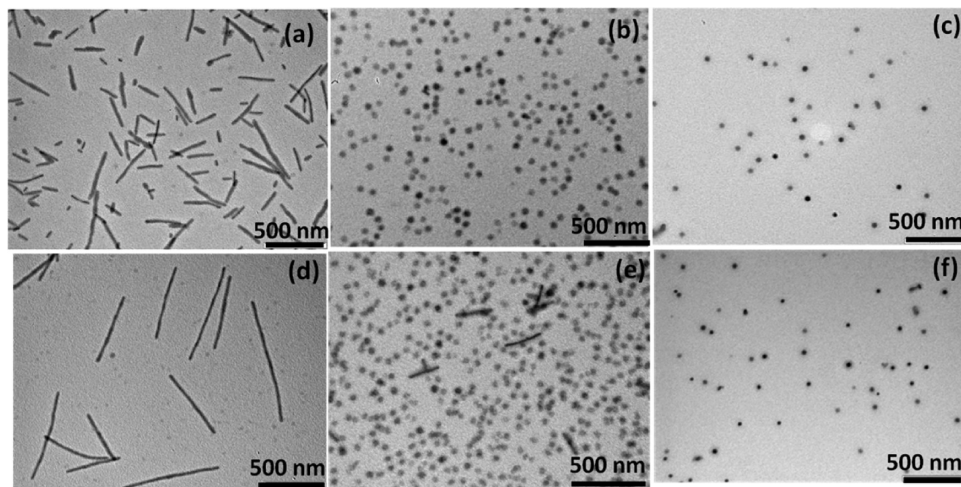


Figure 1. Micelle morphologies of three different $\text{PFS}_x\text{-}b\text{-}\text{P2VP}_{6x}$ diblock copolymers in isopropanol ($i\text{-PrOH}$) at 27°C for 12 h (a, b, c), and at 64°C for 1 h (d, e, f) followed by cooling to 27°C . TEM results showed the $\text{PFS}_{44}\text{-}b\text{-}\text{P2VP}_{264}$ formed cylindrical micelles (a, d), the $\text{PFS}_{75}\text{-}b\text{-}\text{P2VP}_{454}$ formed spherical micelles at 27°C (b), but formed coexisting cylindrical and spherical micelles at 64°C for 1 h (e), and the $\text{PFS}_{102}\text{-}b\text{-}\text{P2VP}_{625}$ formed exclusively spherical micelles at the two different temperatures (c, f).

room temperature (27°C) and, in the case of 64°C , to be slightly below the boiling point of THF (66°C) in order to avoid substantial solvent loss. The results from TEM analysis after solvent evaporation are shown in Figure 1. After 12 h at 27°C the lower molecular weight $\text{PFS}_{44}\text{-}b\text{-}\text{P2VP}_{264}$ sample formed cylindrical micelles of width ca. 33 nm in $i\text{-PrOH}$ (Figure 1a). However, interestingly, exclusively spherical micelles, presumably consisting of the PFS cores and the P2VP coronal layers, were observed for both the medium and higher molecular weight samples, $\text{PFS}_{75}\text{-}b\text{-}\text{P2VP}_{454}$ and $\text{PFS}_{102}\text{-}b\text{-}\text{P2VP}_{625}$, respectively (Figures 1b and 1c). In these images the spherical objects represent only the electron dense PFS core-forming domains, and the corona was not detected due to insufficient contrast with the carbon film used as substrate (a similar situation exists for the other morphologies described in subsequent experiments). The average diameter of the PFS core in the spheres shown in Figures 1b and 1c was 15 nm for $\text{PFS}_{75}\text{-}b\text{-}\text{P2VP}_{454}$ and 16 nm for $\text{PFS}_{102}\text{-}b\text{-}\text{P2VP}_{625}$, respectively. In addition, the size of the spherical micelles including the solvent swollen P2VP coronal layers was found to be approximately 34 and 36 nm, respectively, by DLS (see Figure 4a).

The micellar morphologies for the three different $\text{PFS}_x\text{-}b\text{-}\text{P2VP}_{6x}$ samples in $i\text{-PrOH}$ after heating at 64°C for 1 h followed by cooling to 27°C were also analyzed by TEM (Figure 1d–f). This once again showed the presence of cylinders (widths = ca. 34 nm) for the lower molecular weight $\text{PFS}_{44}\text{-}b\text{-}\text{P2VP}_{264}$ sample (Figure 1d). However, further experiments indicated that cylinders were already present within 10 min of heating at 64°C (Figure S5a) whereas coexisting spherical and cylindrical micelles were formed after 10 min at 27°C (Figure S6a). This indicated for the $\text{PFS}_{44}\text{-}b\text{-}\text{P2VP}_{264}$ sample the rate of the micellar sphere-to-cylinder transition was significantly increased by raising the temperature. In contrast to this behavior, only a few short cylindrical micelles (width = 34 nm) were formed for the medium molecular weight $\text{PFS}_{75}\text{-}b\text{-}\text{P2VP}_{454}$ sample at 64°C after 1 h, and these coexisted with spherical micelles (Figure 1e). Moreover, exclusively spherical micelles were still present after 1 h at 64°C for the high molecular weight $\text{PFS}_{102}\text{-}b\text{-}\text{P2VP}_{625}$ sample (Figure 1f).

In order to investigate whether further transformation of spheres to cylinders would take place in $i\text{-PrOH}$ for the medium

molecular weight $\text{PFS}_{75}\text{-}b\text{-}\text{P2VP}_{454}$ sample at 27°C , the morphology was compared by TEM immediately after heating at 64°C for 1 h and also after subsequently leaving the cooled solution at 27°C for 47 days (Figure 2a,b). A similar, coexisting

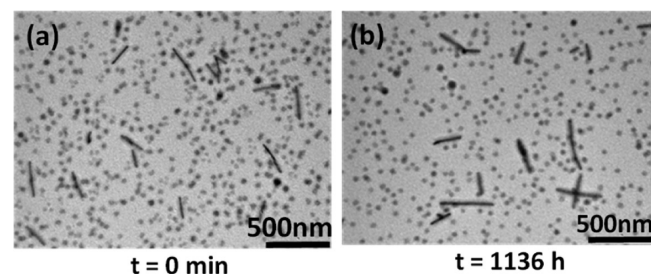


Figure 2. TEM analysis showing coexisting spherical and cylindrical structures were formed for $\text{PFS}_{75}\text{-}b\text{-}\text{P2VP}_{454}$ after heating at 64°C for 1 h and then analyzed by TEM (a) immediately after cooling to room temperature and (b) after a further 47 days at 27°C .

sphere and cylinder micelle morphology was detected in each case, and significantly, both the length of the cylindrical micelles (ca. 200–300 nm) and the ratio of cylinders to spherical micelles were the same within experimental error. This confirmed that the micellar sphere-to-cylinder transition only occurred in $i\text{-PrOH}$ at 64°C for $\text{PFS}_{75}\text{-}b\text{-}\text{P2VP}_{454}$ sample. In the case of the higher molecular weight $\text{PFS}_{102}\text{-}b\text{-}\text{P2VP}_{625}$ sample, spherical micelles were still exclusively present even after heating at 64°C for 1 h and then leaving the solution at 27°C for up to 30 days (Figure S7). These results indicated that, as with the medium molecular weight analogue, the $\text{PFS}_{102}\text{-}b\text{-}\text{P2VP}_{625}$ sample is resistant to the sphere-to-cylinder transition at 27°C , and both apparently remain in a kinetically trapped spherical micelle morphology.^{75,76}

Figures 1a–c show that the molecular weight significantly affects the self-assembly behavior of $\text{PFS}_x\text{-}b\text{-}\text{P2VP}_{6x}$ diblock copolymers in $i\text{-PrOH}$ at 27°C . Only spherical micelles were observed for the medium molecular weight $\text{PFS}_{75}\text{-}b\text{-}\text{P2VP}_{454}$ and high molecular weight $\text{PFS}_{102}\text{-}b\text{-}\text{P2VP}_{625}$ whereas cylindrical micelles were formed for the lower molecular weight $\text{PFS}_{44}\text{-}b\text{-}\text{P2VP}_{264}$ sample. Interestingly, cylindrical micelles appeared to form from spheres at 64°C for the $\text{PFS}_{75}\text{-}b\text{-}\text{P2VP}_{454}$ sample over

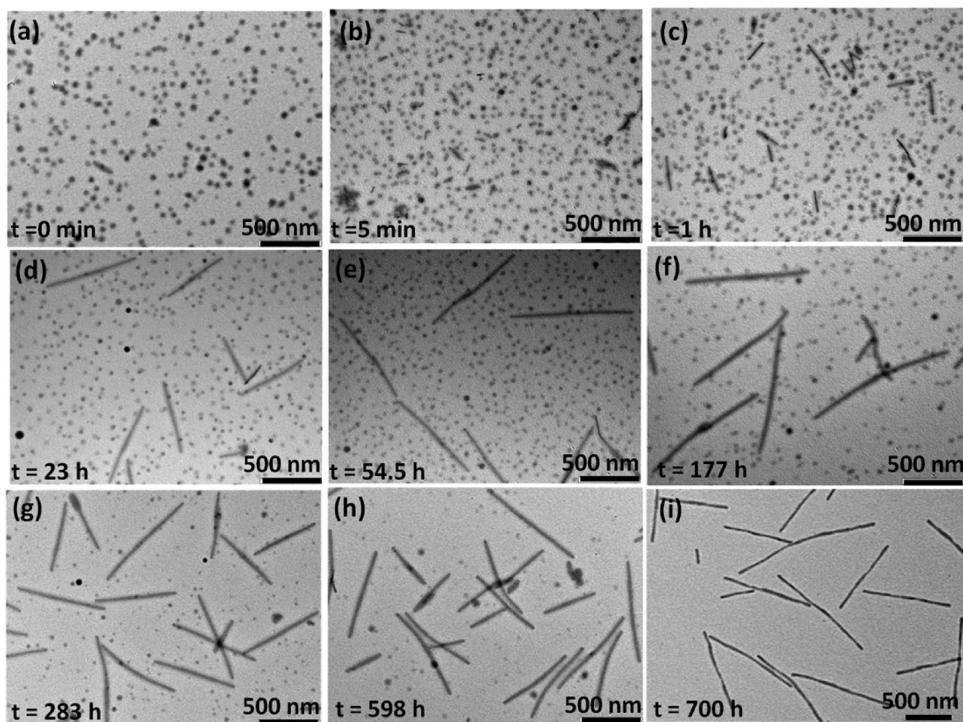


Figure 3. Time-dependent morphological changes for $\text{PFS}_{75}\text{-}b\text{-}\text{P2VP}_{454}$ micelles in i-PrOH at 64°C : (a) exclusively spherical micelles; (b–h) coexisting spherical and cylindrical micelles; (i) exclusively cylindrical micelles. The annealing time is shown in the inset in the figure.

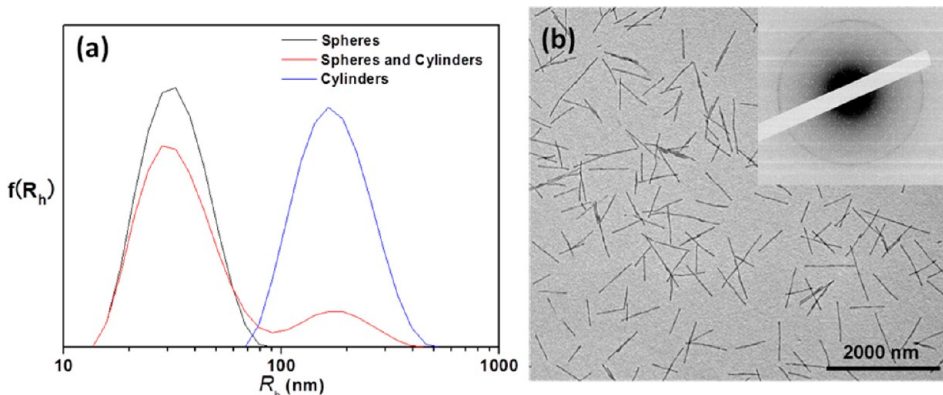


Figure 4. (a) R_{H} distributions of the $\text{PFS}_{75}\text{-}b\text{-}\text{P2VP}_{454}$ micelles in i-PrOH at 64°C for three time intervals by DLS (dark line, $t = 0 \text{ min}$), (red line, $t = 55 \text{ h}$), and (blue line, $t = 700 \text{ h}$). (b) TEM image and a corresponding SAED pattern of the cylindrical $\text{PFS}_{75}\text{-}b\text{-}\text{P2VP}_{454}$ micelles formed in i-PrOH at 64°C after 700 h.

1 h (Figure 1e). Therefore, further experiments were performed to explore the evolution in micellar morphology for different annealing times at 64°C . Figures 3a–i show the time-dependent morphological changes for $\text{PFS}_{75}\text{-}b\text{-}\text{P2VP}_{454}$ in i-PrOH at 64°C . Figure 3a shows the spherical micelles present initially. A few short cylindrical micelles of length 50–100 nm and width ca. 34 nm were already detectable after 5 min. Subsequently, the cylindrical micelles grew steadily over time with a parallel decrease in the numbers of spherical micelles. After 700 h, the micellar sphere-to-cylinder transition was complete, and cylinders of length 600–800 nm were observed (Figure 3i). Once again, we found that the morphology changes detected at 64°C were effectively halted on cooling to 27°C . For example, cooling a sample that had been held at 64°C for 23 h to 27°C for a further 52 h led to no detectable change in morphology (Figure S8).

The morphological transition for $\text{PFS}_{75}\text{-}b\text{-}\text{P2VP}_{454}$ micelles in i-PrOH at 64°C was also monitored *in situ* by DLS experiments. Figure 4a shows that the hydrodynamic radius (R_{H}) of the spherical micelles increased from 34 nm initially (black line) to give aggregates with an apparent value of $R_{\text{H}} = 192 \text{ nm}$ after 700 h (blue line), consistent with the micellar sphere-to-cylinder transition indicated by TEM analysis. At intermediate times such as 55 h (red line) two peaks were present which was consistent with the coexistence of the spherical and cylindrical micelles.

To provide evidence that the formation of the cylindrical micelles from the initially formed spheres in i-PrOH was driven by the crystallization of PFS core-forming metalloblock, selected area electron diffraction (SAED) profiles of spherical and cylindrical micelles were collected respectively (Figure S9b and Figure 4b). The existence of a diffuse ED ring (Figure S9b) from $\text{PFS}_{75}\text{-}b\text{-}\text{P2VP}_{454}$ spheres (Figure S9a) confirmed that the PFS

Table 2. Micelle Morphologies and Approximate Time for Completion of the Micellar Sphere-to-Cylinder Transition for Three Different $\text{PFS}_x\text{-}b\text{-}\text{P2VP}_{6x}$ Diblock Copolymers in i-PrOH at 27 °C or 64 °C, Respectively

	$\text{PFS}_{44}\text{-}b\text{-}\text{P2VP}_{264}$		$\text{PFS}_{75}\text{-}b\text{-}\text{P2VP}_{454}$		$\text{PFS}_{102}\text{-}b\text{-}\text{P2VP}_{625}$
temperature (°C)	27	64	27	64	27
time ^a (h)	5.5	0.1	— ^b	700	— ^b
length (nm)	290	490	— ^b	760	— ^b
length polydispersity	1.06	1.03	— ^b	1.03	— ^b
micelle ^a morphology	cylinders	cylinders	spheres	cylinders	spheres

^aFrom TEM experiments. ^bMicellar sphere-to-cylinder transition did not take place.

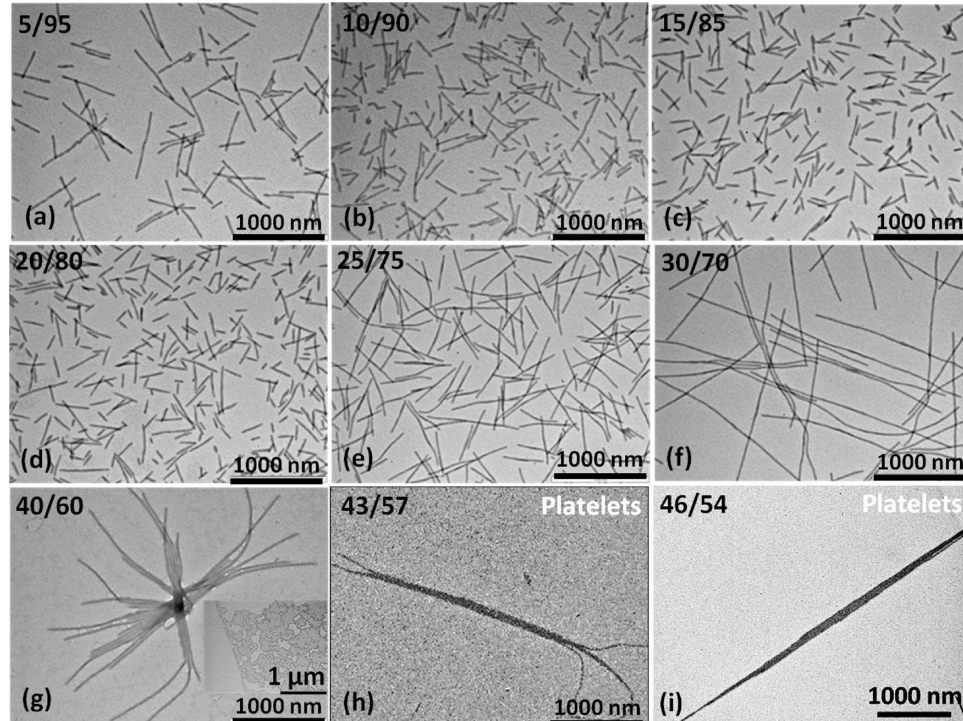


Figure 5. Morphological changes for the $\text{PFS}_{44}\text{-}b\text{-}\text{P2VP}_{264}$ micelles in THF/i-PrOH mixed solutions with increasing THF volume fraction after heating at 64 °C for 1 h and then leaving at 27 °C for 12 h: (a–f) cylindrical micelles; (g) a flower-like cylindrical micelle aggregate and a diblock copolymer film (g, inset); (h, i) a sparse population of narrow lenticular platelet-like micelles. The mixed solvent ratio of THF to i-PrOH (THF/i-PrOH (v/v)) is shown in the figure.

core was in an essentially amorphous state. In contrast, the SAED pattern of the cylindrical $\text{PFS}_{75}\text{-}b\text{-}\text{P2VP}_{454}$ micelles (Figure 4b) showed a strong diffraction ring with $d = 6.0 \text{ \AA}$, confirming that the PFS cores in the cylindrical micelles were in a crystalline state. These results are consistent with the postulate that the micellar sphere-to-cylinder transition was driven by the crystallization of the PFS core, as suggested previously in related but more asymmetric PFS-*b*-P2VP materials based on wide-angle X-ray diffraction data.^{68,70}

Significantly, for the $\text{PFS}_{102}\text{-}b\text{-}\text{P2VP}_{625}$ sample, the initially formed spherical micelles were still stable even after the annealing time at 64 °C reached 183 h (Figure S10). This suggested that crystallization of the PFS core did not take place in i-PrOH under these conditions for this high molecular weight sample and spherical micelles were frozen in a kinetically robust metastable state.^{75,76} The micelle morphologies and the approximate time for completion of the micellar sphere-to-cylinder transition for three different $\text{PFS}_x\text{-}b\text{-}\text{P2VP}_{6x}$ samples in i-PrOH at 27 or 64 °C are summarized in Table 2.

3. Influence of Solvent Selectivity on the Morphology of $\text{PFS}_x\text{-}b\text{-}\text{P2VP}_{6x}$ Micelles.

The influence of solvent selectivity

on the solution self-assembly of three asymmetric $\text{PFS}_x\text{-}b\text{-}\text{P2VP}_{6x}$ samples was explored by characterization of the micellar morphologies formed in these solvent mixtures containing different ratios of a common solvent for both blocks (THF) and the selective solvent for the P2VP corona-forming block used in earlier experiments (i-PrOH). The mixed solvent ratios of THF to i-PrOH studied were from 5/95 through to 50/50 (vol/vol %) corresponding to THF volume fractions (f_{THF}) of 0.05–0.50. The concentration was 0.16 g/L. To rapidly dissolve the samples in the mixed solvent, the $\text{PFS}_x\text{-}b\text{-}\text{P2VP}_{6x}$ solutions were sonicated at 27 °C for 5 min, and these solutions were then heated at 64 °C for 1 h and subsequently cooled to 27 °C for 12 h. The micellar morphologies of the $\text{PFS}_x\text{-}b\text{-}\text{P2VP}_{6x}$ samples were analyzed by TEM, and the morphological changes at different THF volume fractions are shown in Figure 5 ($\text{PFS}_{44}\text{-}b\text{-}\text{P2VP}_{264}$), Figure 6 ($\text{PFS}_{75}\text{-}b\text{-}\text{P2VP}_{454}$), and Figure 7 ($\text{PFS}_{102}\text{-}b\text{-}\text{P2VP}_{625}$). It is significant to note that similar micellar morphologies were obtained for the three $\text{PFS}_x\text{-}b\text{-}\text{P2VP}_{6x}$ diblock copolymers solutions at varied THF volume fractions without the 1 h heating step at 64 °C but over a longer time period (27 h) at 27 °C (Figure S14).

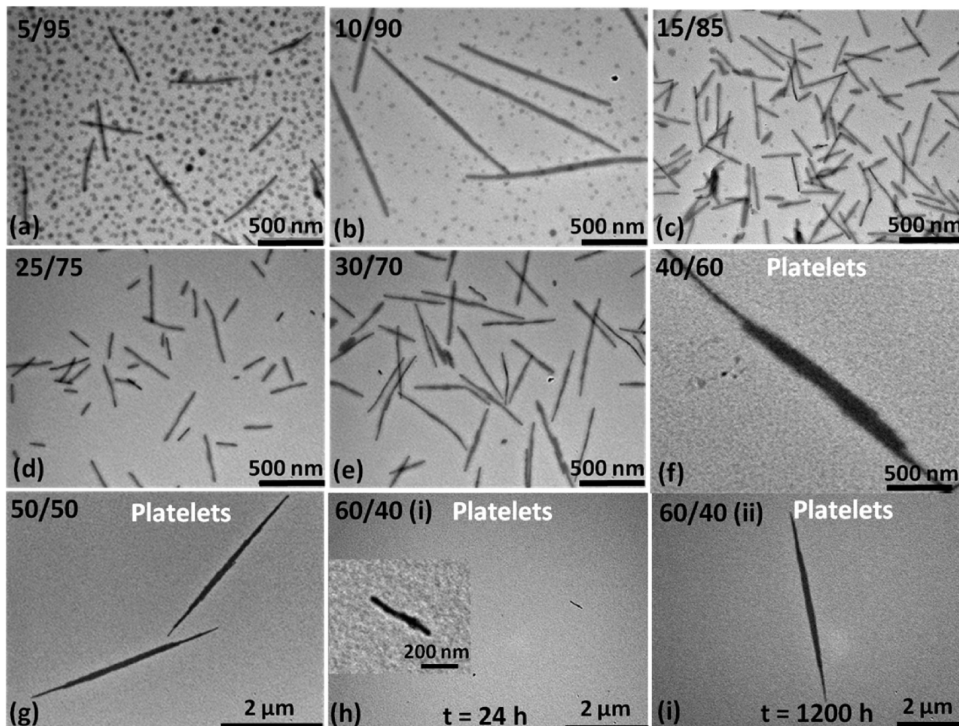


Figure 6. Micelles of the $\text{PFS}_{75}\text{-}b\text{-P2VP}_{454}$ formed in different THF/i-PrOH mixed solutions at 27°C for 24 h (a–h) and 1200 h (i) after heating at 64°C for 1 h initially. (a, b) Coexisting sphere and cylinder micelles; (c–e) cylindrical micelles; (f–i) narrow lenticular-shaped platelet micelles. (h) A small lenticular platelet grown at 27°C over 24 h, and (i) a large lenticular-shaped platelet formed at 27°C over 1200 h. An inset in (h) includes an enlarged lenticular platelet. THF/i-PrOH (v/v) values are shown in the figure.

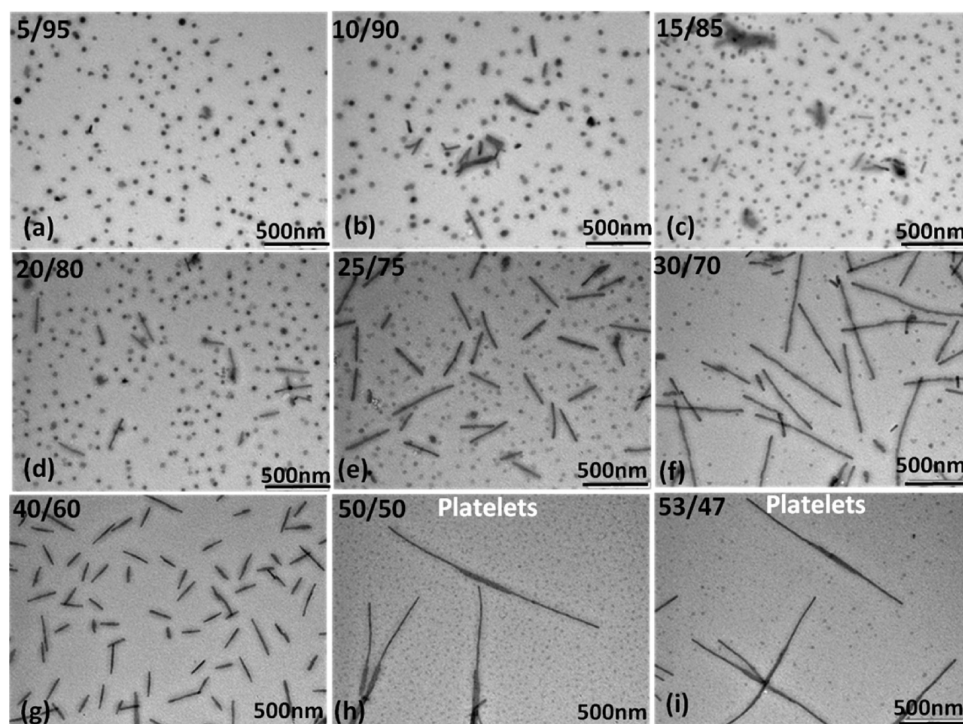


Figure 7. Micellar sphere-to-cylinder-to-platelet transition for the $\text{PFS}_{102}\text{-}b\text{-P2VP}_{625}$ diblock copolymer in THF/i-PrOH mixed solvent with increasing THF fraction after heating at 64°C for 1 h and then leaving at 27°C for 24 h: (a) spherical micelles; (b–f) coexisting spherical and cylindrical micelles; (g) short cylindrical micelles; (h, i) narrow lenticular platelet micelles and the aggregates. The THF/i-PrOH blending ratio is shown in each figure.

For the self-assembly of the lower molecular weight $\text{PFS}_{44}\text{-}b\text{-P2VP}_{264}$ sample in $\text{THF}/\text{iPrOH} = 5/95$ ($f_{\text{THF}} = 0.05$) cylindrical micelles of length ca. 480 nm were formed (Figure 5a). When

f_{THF} was further increased to 0.10, the cylindrical micelles significantly decreased in length to ca. 200–400 nm and increased in number (Figure 5b). This decrease in the size of

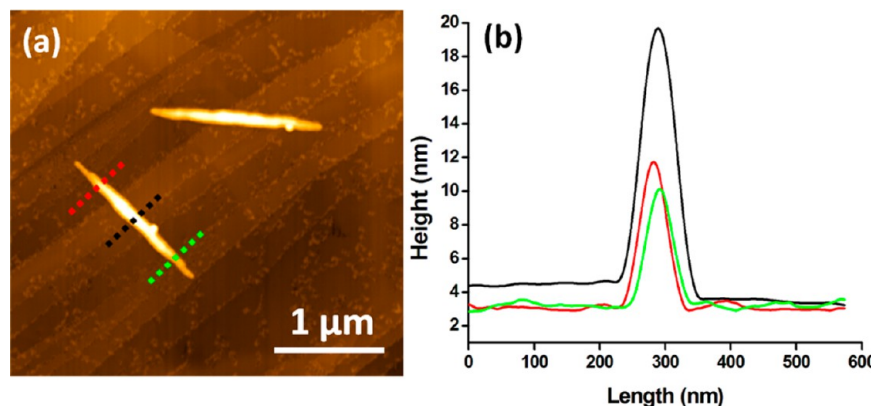


Figure 8. (a) AFM image of an isolated narrow lenticular PFS_{102} -*b*- P2VP_{625} platelet micelle observed using the height mode. (b) Height profiles of the narrow lenticular platelet collected in three different paths.

the cylinders after an increase in the concentration of common solvent was probably caused by a solvent induced fragmentation effect as found previously in related systems.^{77,78} Cylindrical micelles of similar length were observed at $f_{\text{THF}} = 0.15$ and 0.20 (Figures 5c and 5d, respectively). Interestingly, a significant increase in length of cylindrical micelles from ca. 550 nm to ca. 1800 nm was observed at $f_{\text{THF}} = 0.25$ and 0.30 , respectively (Figures 5e and 5f). In all of these cases (in Figures 5a–f) the width of the PFS core measured by TEM was constant at ca. 30 nm. When f_{THF} was further increased to 0.40 , however, only a few aggregates of cylindrical micelles were detected (Figure 5g), and most of the sample appeared to be in a dissolved state as a film was formed on solvent evaporation (Figure 5g, inset). Interestingly, platelet micelles of maximum width ca. 130 nm were formed at f_{THF} larger than 0.4 , and they possessed rough and curved edges (Figures 5h,i).

Next, the micellar morphology transformations for the medium molecular weight of PFS_{75} -*b*- P2VP_{454} in THF/i-PrOH were studied as a function of f_{THF} . The morphological changes as the f_{THF} value increased from 0.05 to 0.60 are shown in Figures 6a–i. In contrast to the formation of exclusively cylindrical micelles for low molecular weight PFS_{44} -*b*- P2VP_{264} at $f_{\text{THF}} = 0.05$, coexisting micelle morphologies consisting of spheres and short (ca. 500 nm) cylinders were observed under the same conditions (Figure 6a). When the f_{THF} was further increased to 0.10 , a decrease in the amount of spherical micelles and an associated increase in the length of the cylindrical micelles was observed (Figure 6b).

At $f_{\text{THF}} = 0.15$, 0.25 , and 0.30 exclusively cylindrical micelles were observed (Figures 6c–e), a striking difference to the situation in pure i-PrOH where the sphere-to-cylinder transformation did not take place even at 27°C after 47 days (Figure 2). This indicated that the addition of THF as a common solvent to the i-PrOH selective solvent clearly accelerated the rate of the micellar sphere-to-cylinder transition, and in this process THF functions as a “catalyst”. Interestingly, at $f_{\text{THF}} = 0.4$ elongated platelet micelles were detected (Figure 6f). When the f_{THF} was further increased to 0.5 , exclusively platelet micelles were observed, and these were “narrow lenticular” shaped objects with rough and curved edges (Figure 6g). Significantly, coexisting sphere and small lenticular platelet micelles were observed when the solution was cooled to 27°C for 2 h (Figure S12). This indicated that the micellar transition from spheres to platelets occurred in the solution at $f_{\text{THF}} = 0.50$. When f_{THF} further increased to 0.60 , only a few tiny narrow lenticular

platelet micelles were observed (Figure 6h). Similar sized platelet micelles were observed in both Figure 6g and 6i, but they were formed over different growth periods (12 and 1200 h).

DLS experiments on micelles formed by PFS_{75} -*b*- P2VP_{454} at medium and high THF volume fractions were also performed (Figure S11). In comparison to the R_H value found for the spherical micelles (34 nm), the DLS results showed a substantial increase in the apparent hydrodynamic radius micelle at medium (Figure S11a, apparent $R_{H,\text{app}} = 91$ nm) and high THF values (Figure S11b, $R_{H,\text{app}} = 600$ nm). This is consistent with the presence of cylindrical micelles at $f_{\text{THF}} = 0.30$ and platelets at $f_{\text{THF}} = 0.50$ detected by TEM analysis.

A TEM image and a corresponding SAED pattern for two irregular-shaped, narrow lenticular PFS_{75} -*b*- P2VP_{454} platelet micelles formed at $f_{\text{THF}} = 0.50$ are shown in Figures S13a and S13b, respectively. The appearance of several ED rings in Figure S13b provided evidence that these platelets also possessed crystalline PFS cores, as found previously⁷² for such structures generated from PFS-*b*-P2VP block copolymers with 1:1 or 5:1 block ratios.

Finally, the morphology of the micelles formed by higher molecular weight PFS_{102} -*b*- P2VP_{625} was explored under different solvent conditions corresponding to $f_{\text{THF}} = 0.05$ – 0.53 (Figure 7). These diblock copolymer solutions were analyzed by TEM after heating at 64°C for 1 h and then left at 27°C for 12 h, and a micellar sphere–cylinder–platelet transition was detected again by the increase in f_{THF} value. Exclusively spherical micelles were observed at $f_{\text{THF}} = 0.05$ (Figure 7a). The fraction of cylindrical micelles was found to gradually increase at the expense of spherical micelles when the f_{THF} increased from 0.10 to 0.30 (Figures 7b–f). Only cylindrical micelles with a length of ca. 275 nm were formed at $f_{\text{THF}} = 0.4$ (Figure 7g), and aggregated narrow lenticular-shaped platelet micelles were detected when the f_{THF} increased to ca. 0.50 (Figures 7h,i).

In order to provide further characterization of the narrow lenticular platelet morphology, a representative example of a PFS_{102} -*b*- P2VP_{625} platelet micelle was examined by tapping mode AFM (Figure 8). The total thickness of this platelet was small ($d_{(\text{PFS+P2VP})} = 10$ – 20 nm, Figure 8b), which is indicative of a very thin crystalline nanostructure. Furthermore, height profiles of the center and the two ends of a narrow lenticular platelet indicated that the thickness of the former (~ 14 – 15 nm) is significantly larger than that of the latter (~ 8 nm) (Figure 8b). The thick center portion of the platelet is attributed to the contribution from a seed nucleus in the crystalline PFS core in

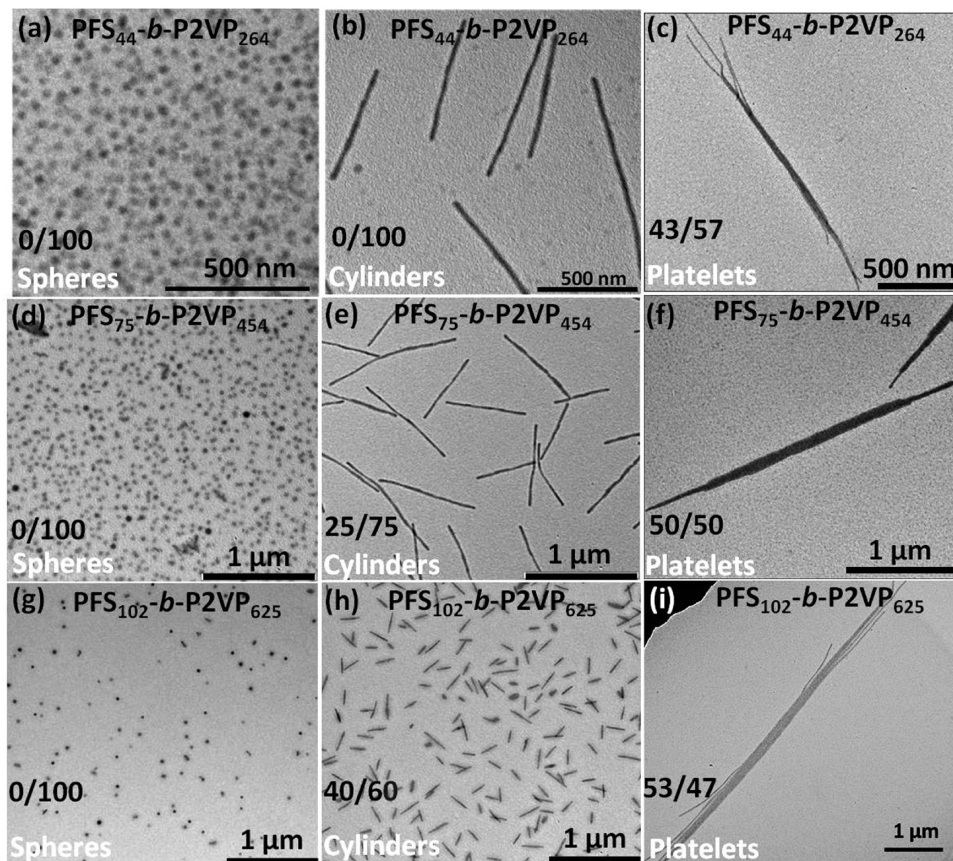


Figure 9. Micellar sphere-to-cylinder-to-platelet transitions for the three $\text{PFS}_x\text{-}b\text{-}\text{P2VP}_{6x}$ samples in THF/i-PrOH mixed solvents by increasing the THF fraction after heating at 64°C for 1 h and then leaving the samples at 27°C for 24 h (b–i). Spherical micelles (a, d, g), cylindrical micelles (b, e, h), and platelet micelles (c, f, i) were observed. (a) Spherical $\text{PFS}_{44}\text{-}b\text{-}\text{P2VP}_{264}$ micelles were formed initially in i-PrOH at 27°C for 1 min. $\text{PFS}_x\text{-}b\text{-}\text{P2VP}_{6x}$ and THF/i-PrOH ratios are shown in each figure.

the platelet.^{76,90} The AFM and TEM data are consistent with a picture where the narrow lenticular thin platelet micelles consist of a crystalline, chain-folded PFS core covered by two glassy P2VP layers ($T_g^{\text{P2VP}} = 104^\circ\text{C}$).^{72,79}

The studies in THF/i-PrOH indicated that micellar sphere-to-cylinder-to-platelet transitions could also be induced by the addition of THF to i-PrOH for $\text{PFS}_{102}\text{-}b\text{-}\text{P2VP}_{625}$, in contrast to heating at 64°C for 183 h in pure i-PrOH which led to no detectable change to the spherical morphology initially observed. THF therefore played a “catalytic” role as it was able to induce morphological changes for the three asymmetric $\text{PFS}_x\text{-}b\text{-}\text{P2VP}_{6x}$ block copolymer micelles in THF/i-PrOH mixed solvents. Figure 9 summarizes the morphological behavior for the three $\text{PFS}_x\text{-}b\text{-}\text{P2VP}_{6x}$ diblock copolymer samples with different overall molecular weights on increasing the ratio of THF to i-PrOH. Micellar sphere-to-cylinder-to-platelet transitions were observed for three asymmetric $\text{PFS}_x\text{-}b\text{-}\text{P2VP}_{6x}$ samples in mixed THF/i-PrOH mixed solvents.

4. Selected Area Electron Diffraction Studies on Cylindrical and Platelet $\text{PFS}_x\text{-}b\text{-}\text{P2VP}_{6x}$ Micelles. *a. Studies of Cylindrical Micelles.* To analyze the crystalline PFS cores of cylinder and platelet micelles in more detail, selected area electron diffraction (SAED) patterns were collected for ordered cylindrical and platelet $\text{PFS}_{75}\text{-}b\text{-}\text{P2VP}_{454}$ micelles. Previous work on electric-field-aligned monodisperse cylinders formed by PFS-*b*-PI block copolymers with a short PFS block using synchrotron X-ray scattering data indicated the presence of aligned cylindrical micelles with single crystal type order.⁸⁰ We identified three

cylindrical $\text{PFS}_{75}\text{-}b\text{-}\text{P2VP}_{454}$ micelles having a similar, almost parallel orientation by TEM analysis (Figure 10a) and obtained an SAED pattern (Figure 10b).⁸¹ Significantly, a spot-type ED pattern was detected from these oriented cylindrical micelles (Figure 10b) which indicated that the crystalline PFS core of the $\text{PFS}_{75}\text{-}b\text{-}\text{P2VP}_{454}$ cylinders also exists a state reminiscent of a single crystal. Furthermore, the ED pattern shown in Figure 10b, which includes three pairs of ED spots separated by about 60° , is

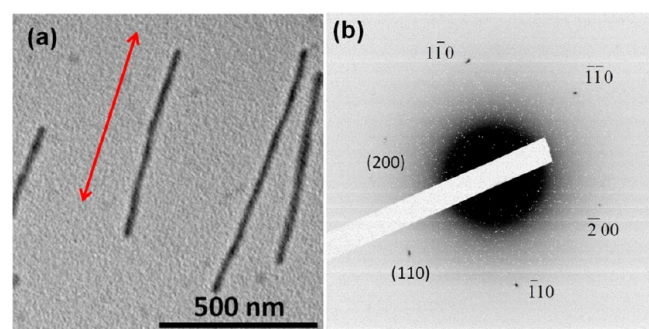


Figure 10. (a) Three ordered cylindrical micelles of $\text{PFS}_{75}\text{-}b\text{-}\text{P2VP}_{454}$ formed in i-PrOH and a red double arrow line represents the two growth directions of three cylindrical micelles. (b) A spot-type SAED pattern was collected from these oriented cylindrical micelles. The SAED pattern includes three pairs of ED spots separated by about 60° which indicates that crystalline PFS core in these cylinder micelles exists in a single crystalline state.

virtually identical to a SAED pattern previously collected from a rectangular crystalline PI-*b*-PFS platelet.³⁷ According to the results for PFS crystals with a monoclinic unit cell in electrospun nanofibers reported by Manners, Foster, and Reneker et al. ($a = 14.20 \text{ \AA}$, $b = 6.03 \text{ \AA}$, $c = 13.9 \text{ \AA}$, and $\gamma = 95.1^\circ$),⁸² the data in Figure 10b were assigned as a [001] zone ED pattern for PFS single crystals. In Figure 10b, one pair of ED spots with a *d*-spacing of 0.5973 nm was indexed as a set of (200) planes, while the other two pairs of ED spots with a *d*-spacing of 0.5875 nm were assigned to sets of (110) and (110) planes, respectively.^{82,83}

b. Studies of a Narrow Lenticular Platelet Micelle. Narrow lenticular platelet micelles were only observed at high THF volume fractions, and as discussed above, the crystalline nature of the PFS core in the platelets was confirmed by the SAED pattern obtained for two PFS₇₅-*b*-P2VP₄₅₄ platelet micelles (Figure S13b). We also investigated an isolated narrow lenticular platelet with a high aspect ratio (for a TEM image see Figure 11a). The

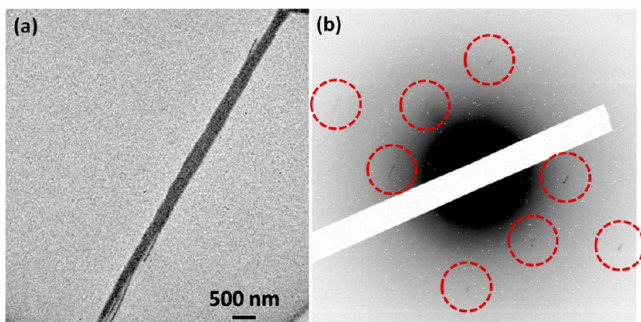


Figure 11. (a) A bright field TEM image and (b) a arc-type SAED pattern of a isolated narrow lenticular PFS₇₅-*b*-P2VP₄₅₄ platelet micelle formed in THF/i-PrOH mixed solvent (50/50 v/v). Eight ED arcs included within the brown dashed line circles are observed in (b). The camera length used for taking this ED pattern was 80 cm. The SAED pattern shows a arc-type pattern which indicates that crystalline PFS core in the narrow lenticular platelet micelles exists in the polycrystalline state.

corresponding SAED pattern of the platelet included four pairs of diffraction arcs (Figure 11b) and confirmed that the PFS was in a *polycrystalline* state. An arc-typed ED pattern showed that the polycrystalline PFS core in a platelet micelle consisted of many PFS microcrystals but with a similar crystal orientation.

DISCUSSION

Previous work has shown that asymmetric PFS-*b*-P2VP block copolymers tend to form spheres with an amorphous PFS core in P2VP-selective alcohols as solvents which gradually transform into cylinders where the core is crystalline. The rate of this crystallization-driven transition to form a morphology with lower mean core–coronal interfacial curvature³⁴ has been shown to increase by the use of a less hydrophilic alcohol, such as i-PrOH compared to MeOH, that is more compatible with the PFS core-forming block. This has been proposed to be a consequence of a solvent plasticization effect that facilitates PFS crystallization by solvent penetration into the core.⁷⁰

In the present study the influence of molar mass at constant block ratio (1:6) on the crystallization-driven micellar sphere-to-cylinder transition in i-PrOH was clearly demonstrated by the TEM and SAED results described. As summarized in Table 2, at 27 °C exclusively cylindrical micelles were observed in i-PrOH for low molecular weight PFS₄₄-*b*-P2VP₂₆₄ whereas spherical micelles with amorphous PFS cores were formed for the medium

molar mass PFS₇₅-*b*-P2VP₄₅₄ and high molar mass PFS₁₀₂-*b*-P2VP₆₂₅ samples. On heating at 64 °C a sphere-to-cylinder transition was induced for the medium molecular weight sample, but for the high molecular weight sample amorphous spheres remained as the only detected morphology, even after heating at this temperature for ca. 180 h. These results can be explained by the crystallization characteristics of the PFS core-forming metalloblock. Previous reports have shown that, perhaps as a result of the bulky ferrocene groups in the main chain, the crystallization of bulk or thin film samples of PFS homopolymer ($T_g = 34 \text{ }^\circ\text{C}$ ⁸⁴ and $T_{m,\text{eq}} = 143 \text{ }^\circ\text{C}$ (Hoffman–Weeks)⁸⁵ or 210 °C (Gibbs–Thomson)⁸⁶) from the melt is characterized by a slow crystal growth rate and the generation of relatively low degrees of crystallinity.^{85,86} Moreover, a further decrease in the rate of the crystallization would be expected with an increase in molecular weight.⁸⁵ Improved chain mobility for the crystallizable PFS block for the low and medium molecular weight samples at 64 °C explains the rapid crystallization-driven transition from spheres to cylinders. However, it is remarkable that rate of crystallization for the high molecular weight sample is still insignificant under these conditions.

The influence of solvent selectivity on micelle morphology for three different PFS_x-*b*-P2VP_{6x} samples was also explored in detail. Interestingly, a micellar sphere-to-cylinder-to-narrow lenticular platelet transition was observed for all three PFS_x-*b*-P2VP_{6x} block copolymers in THF/i-PrOH mixed solvents on increasing the amount of common solvent (THF). The ability to form micelles with different interfacial curvature (spheres, cylinders, or platelets) can be ascribed to the interplay between the crystallization of the core-forming block, which favors extended crystalline cores and flat interfaces, and the repulsion between the corona-forming blocks, which forces the core–coronal interface to curve and thereby confines the lateral growth of the crystalline core.³⁴

It is expected⁷⁰ that THF, a common solvent for both the PFS core and the P2VP coronal-forming blocks, would act as a “plasticizer” to increase the solubility of the crystallizable PFS core-forming block and would facilitate crystallization. This effect on PFS_x-*b*-P2VP_{6x} micelle morphology can be analyzed quantitatively by considering the solubility parameter (δ) of the solvents and blocks. The δ values for THF and i-PrOH are 18.5 and 23.5 MPa^{1/2}, respectively,⁷⁹ whereas $\delta(\text{PFS}) = 18.7 \text{ MPa}^{1/2}$ and $\delta(\text{P2VP}) = 21.7 \text{ MPa}^{1/2}$. Thus, it is clear that the solvent quality for the PFS core should increase substantially on addition of THF to i-PrOH, reminiscent of the case of the replacement of MeOH ($\delta = 29.7 \text{ MPa}^{1/2}$) by i-PrOH ($\delta = 23.5 \text{ MPa}^{1/2}$) discussed above.^{68,70} Thus, plasticization, which would improve the main chain mobility for the short core-forming PFS metalloblock, should facilitate crystallization and the formation of morphologies with low curvature of the core–corona interface and more extensive lateral growth. Although the detailed mechanism for the morphological transitions is not clear,⁷⁰ this is consistent with the formation of spheres, cylinders, and narrow lenticular platelets as the THF concentration in the THF/i-PrOH mixed solution is increased (see Figure 9 and Figure S14). It should be noted that the effect of facilitating PFS core crystallization may also be complemented by contraction of the coronal coils of the P2VP coronal block, which otherwise limits the lateral growth of the crystalline PFS core, as THF is a significantly poorer solvent for P2VP than i-PrOH. The change in morphological preference from cylinders to platelets under conditions of improved solvation of the core-forming block has been previously noted for other crystalline-coil block copolymers

such as poly(ethylene-*b*-butadiene) (PEO-*b*-PB) and poly(isoprene-*b*-ferrocenyldiethylsilane) (PI-*b*-PFDES) systems.^{65,87}

Detailed structural information on the crystalline PFS core within cylindrical PFS_x-*b*-P2VP_{6x} micelles was obtained by comparing the spot-type SAED pattern of ordered PFS_x-*b*-P2VP_{6x} micelles (Figure 10b) to that for a rectangular platelet of PFS-*b*-PI obtained previously. The spot-type [001] zone ED patterns collected from the cylindrical micelles with similar orientations and the PFS-*b*-PI platelet³⁷ were essentially identical. Similar diffraction patterns to those observed were also previously obtained for drawn and electrospun PFS homopolymer nanofibers and monodisperse, electric-field-aligned PFS-*b*-PI cylinders.^{80,82} These results are consistent with the PFS core in the cylindrical micelles existing in an essentially single crystalline state with monoclinic symmetry. Significantly, the presence of the long coronal P2VP block does not appear to affect the structure of the single-crystalline PFS core in these cylindrical structures during the growth process.

The situations where a spot-type [001] zone ED pattern containing six indexed ED spots was collected from the single crystalline core of a rectangular PFS-*b*-PI platelet³⁷ or a cylindrical PFS_x-*b*-P2VP_{6x} micelle are illustrated in Figures 12a

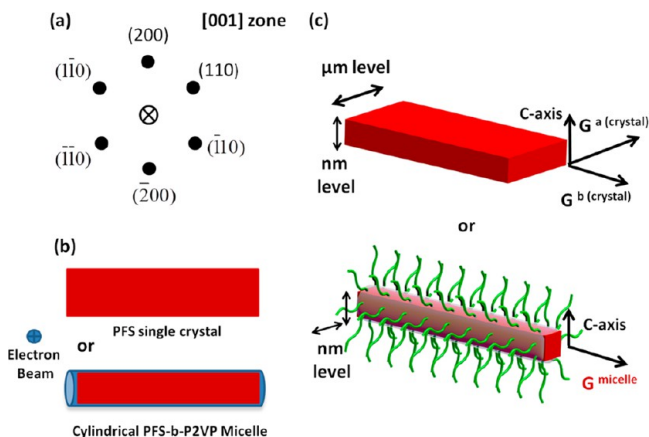


Figure 12. (a) An identical ED pattern including six indexed diffraction spots collected from (b) an illustrated rectangular PFS-*b*-PI platelet or a cylindrical PFS_x-*b*-P2VP_{6x} micelle with a PFS single crystalline core. Covered glassy P2VP layers were not included for clarity. (c) The growth mechanism of a rectangular PFS single crystal and a cylindrical PFS_x-*b*-P2VP_{6x} micelle having a PFS single crystalline core, respectively. G indicates the growth direction of the monoclinic PFS crystal.

and 12b, respectively. The data indicate that the growth of a cylindrical PFS_x-*b*-P2VP_{6x} micelle is driven by the crystallization of PFS along the *b*-axis direction of the single crystalline PFS core. The repulsive interactions between the long P2VP blocks confine the lateral (*a*-axis) growth of the regular PFS single crystalline core on the nanometer scale within a defined cylindrical region of space as a result of the surrounding amorphous P2VP coronal blocks. Figure 12c illustrates how the 1D *b*-axis growth of the crystalline PFS core causes the formation of a elongated cylindrical micelle (the diameter of the cylindrical micelle is on the nanometer level (ca. 25–35 nm), and the length of the cylindrical micelle can reach several micrometers), whereas 2D growth along both the *b*- and *a*-axes would be expected to generate a rectangular platelet on the micrometer scale.

In contrast to systems such as PFS homopolymer,⁸⁸ PFS-*b*-PI,³⁷ and PFS-*b*-PDMS⁸⁹ for which rectangular platelets have been characterized in solution, the PFS_x-*b*-P2VP_{6x} systems in this

study formed narrow lenticular platelet micelles at high THF volume fractions. Moreover, whereas the former platelet micelles have been shown to single crystalline³⁷ and to possess smooth growth fronts, for the latter the core is polycrystalline and the growth fronts are irregular (Figure 13). In general, a crystallizable

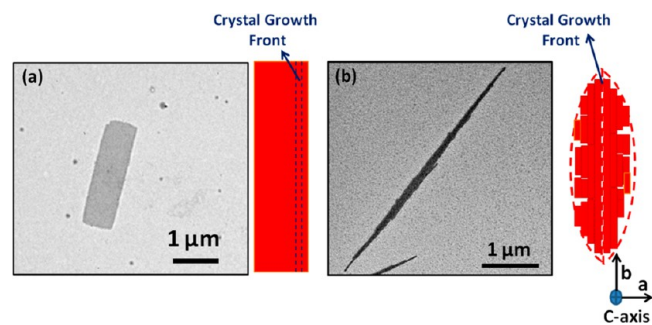


Figure 13. (a) Rectangular PFS₂₂ platelet formed in THF/hexane mixed solvent (50/50 v/v) and a hypothesized growth mechanism of the formation of a rectangular platelet structure having the single crystalline PFS core (top view). (b) Narrow lenticular shaped PFS_x-*b*-P2VP_{6x} platelet micelles formed in THF/i-PrOH mixed solvent (50/50 v/v) (top view) and a hypothesized growth mechanism of the formation of narrow lenticular platelet with the polycrystalline PFS core. Two covered glassy P2VP layers are not illustrated here.

polymer with a low rotational symmetry unit cell such as monoclinic with low helical 2¹ rotational symmetry^{82,83} might be expected to form narrow platelets.^{76,90} The formation of rough edges to the platelets can be attributed to significant interference or “poisoning” on the crystal growth fronts from the long coronal P2VP blocks to introduce defects.⁹¹ Furthermore, this poisoning effect would be expected to change the rates of both secondary nucleation and the radial growth at the crystal growth fronts and lead to the formation of polycrystalline narrow lenticular structures. The influence of poisoning effects on the platelet morphology is further supported by previously studies of the self-assembly of the PFS-*b*-P2VP samples with a crystalline PFS core-forming block of equal length or longer than that of the P2VP segment.⁷² Other examples include the pointed oval-shaped micelles formed by PFS-*b*-PP (PP = polyphosphazene) on addition to PFS-*b*-P2VP seeds in i-PrOH⁹² and the lenticular shaped PS-*b*-PFS (PS = polystyrene) platelets found in dichloromethane when the crystallization of the core PFS blocks took place at a low degree of oxidation (*x* = 0.25).⁹³

SUMMARY

Important further insight into the factors that control micellar morphology during the solution self-assembly of asymmetric crystalline-coil block copolymers has been obtained from the study of PFS-*b*-P2VP block copolymers under conditions where micelles with a PFS core are formed. The effect of molar mass and solvent selectivity on the resulting micelle morphologies and morphological transitions was explored for three different PFS_x-*b*-P2VP_{6x} samples with the same block ratio but different molar masses. The results showed the rate of the micellar sphere-to-cylinder transition in i-PrOH is significantly decreased by an increase in the overall molar mass of the PFS_x-*b*-P2VP_{6x} diblock copolymer.

Changing the solvent quality by the addition of the common solvent THF to the i-PrOH slightly improved the solubility of the PFS core-forming block and facilitated crystallization, presumably via a plasticization effect. As the THF volume fraction

increased, the favored morphology changed from spheres, with an amorphous PFS core, to cylinders and then to narrow lenticular platelets, with crystalline PFS cores. SAED results confirmed that the PFS core within the cylindrical micelles was reminiscent of a single crystal with a monoclinic structure and that cylinder formation appears to involve growth along the crystallographic *b*-axis of the single crystalline PFS core. In contrast, the narrow lenticular platelets were shown to possess a polycrystalline PFS core. The formation of platelet structures with rough edges, rather than the rectangular micelles with smooth edges observed in other systems, was attributed to a poisoning effect arising from the interference of the P2VP coronal blocks with the growth fronts of the PFS core.

■ ASSOCIATED CONTENT

Supporting Information

Experimental details and additional experimental results. This material is available free of charge via the Internet at <http://pubs.acs.org>.

■ AUTHOR INFORMATION

Corresponding Authors

*E-mail ian.manners@bristol.ac.uk (I.M.).

*E-mail mwinnik@chem.utoronto.ca (M.A.W.).

Present Addresses

[§]M.-S.H.: UES, Inc. and Materials & Manufacturing Directorate, Air Force Research Laboratory, WPAFB, OH 45433.

^{||}S.F.M.Y.: Universiti Kebangsaan Malaysia, 43600 UKM Bangi, Selangor, Malaysia.

Notes

The authors declare no competing financial interest.

■ ACKNOWLEDGMENTS

M.-S.H. thanks the EU for a Marie Curie Fellowship. S.F.M.Y. is grateful to the Ministry of Higher Education of Malaysia and Universiti Kebangsaan Malaysia for the provision of a Ph.D scholarship. I.M. thanks the EU for a Marie Curie Chair and the European Research Council for an Advanced Investigator Grant. M.A.W. also thanks NSERC of Canada for financial support.

■ REFERENCES

- Bates, F. S. *Science* **1991**, *251*, 898–905.
- Hamley, I. W. *The Physics of Block Copolymers*; Oxford University Press: New York, 1998.
- Förster, S.; Antonietti, M. *Adv. Mater.* **1998**, *10*, 195–217.
- Förster, S.; Plantenberg, T. *Angew. Chem., Int. Ed.* **2002**, *41*, 688–714.
- Schacher, F. H.; Rupar, P. A.; Manners, I. *Angew. Chem., Int. Ed.* **2012**, *51*, 7898–7921.
- Alexandridis, P.; Lindman, B. *Amphiphilic Block Copolymers: Self-Assembly Ed.*; Elsevier: New York, 2000.
- Klok, H. A.; Lecommandoux, S. *Adv. Mater.* **2001**, *13*, 1217–1229.
- Krausch, G.; Magerle, R. *Adv. Mater.* **2002**, *14*, 1579–1583.
- Discher, D. E.; Eisenberg, A. *Science* **2002**, *297*, 967–973.
- Park, C.; Yoon, J.; Thomas, E. L. *Polymer* **2003**, *44*, 6725–6760.
- Cheng, J. Y.; Mayes, A. M.; Ross, C. A. *Nat. Mater.* **2004**, *3*, 823–828.
- Hamley, I. W. *Block Copolymers in Solution: Fundamentals and Applications*; John Wiley & Sons Ltd.: Chichester, 2005.
- Halperin, A.; Tirrell, M.; Lodge, T. P. *Adv. Polym. Sci.* **1991**, *100*, 31.
- Rodriguez, J.; Checot, F.; Gnanou, Y. L.; Lecommandoux, G. S. *Prog. Polym. Sci.* **2005**, *30*, 691–724.
- Mahanthappa, M.; Lim, L. S.; Hillmyer, M. A.; Bates, F. S. *Macromolecules* **2007**, *40*, 1585–1593.
- Cao, L.; Massey, J. A.; Winnik, M. A.; Manners, I.; Riethmuller, S.; Banhart, F.; Möller, M. *Adv. Funct. Mater.* **2003**, *13*, 271–276.
- Lazzari, M.; Rodriguez-Abreu, C.; Rivas, J.; Lopez-Quintela, M. A. *J. Nanosci. Nanotechnol.* **2006**, *6*, 892–905.
- Korczagin, I.; Hempenius, M. A.; Fokkink, R. G.; Stuart, M. A. C.; Al-Hussein, M.; Bomans, P. H. H.; Frederik, P. M.; Vancso, G. J. *Macromolecules* **2006**, *39*, 2306–2315.
- Vandermeulen, G. W. M.; Kim, K. T.; Wang, Z.; Manners, I. *Biomacromolecules* **2006**, *7*, 1005–1010.
- Lau, K. H. A.; Bang, J.; Kim, D. H.; Knoll, W. *Adv. Funct. Mater.* **2008**, *18*, 3148–3157.
- Qian, J.; Zhang, M.; Manners, I.; Winnik, M. A. *Trends Biotechnol.* **2010**, *28*, 84–92.
- Zhang, L.; Eisenberg, A. *Science* **1995**, *268*, 1728–1731.
- Zhang, L.; Yu, K.; Eisenberg, A. *Science* **1996**, *272*, 1777–1779.
- Zhang, L. F.; Eisenberg, A. *J. Am. Chem. Soc.* **1996**, *118*, 3168–3181.
- Yu, K.; Eisenberg, A. *Macromolecules* **1998**, *31*, 3509–3518.
- Lotz, B.; Kovacs, A. *J. Colloid Polym. Sci.* **1966**, *209*, 97–114.
- Lotz, B.; Kovacs, A. J.; Bassett, G. A.; Keller, A. *Kolloid Z. Z. Polym.* **1966**, *209*, 115.
- Kovacs, A. J.; Lotz, B.; Keller, A. *J. Macromol. Sci., Phys.* **1969**, *B3* (3), 385.
- Lin, E. K.; Gast, A. P. *Macromolecules* **1996**, *29*, 4432.
- Hsiao, M. S.; Chen, W. Y.; Zheng, J. X.; Van Horn, R. M.; Quirk, R. P.; Ivanov, D. A.; Thomas, E. L.; Lotz, B.; Cheng, S. Z. D. *Macromolecules* **2008**, *41*, 4794–4801.
- Hsiao, M. S.; Zheng, J. X.; Leng, S. W.; Van Horn, R. M.; Quirk, R. P.; Thomas, E. L.; Chen, H. L.; Hsiao, B. S.; Rong, L. X.; Lotz, B.; Cheng, S. Z. D. *Macromolecules* **2008**, *41*, 8114–8123.
- Hsiao, M. S.; Zheng, J. X.; Van Horn, R. M.; Quirk, R. P.; Thomas, E. L.; Chen, H. L.; Lotz, B.; Cheng, S. Z. D. *Macromolecules* **2009**, *42*, 8343–8352.
- Whittell, G. R.; Hager, M. D.; Schubert, U. S.; Manners, I. *Nat. Mater.* **2011**, *10*, 176–188.
- Massey, J. A.; Temple, K.; Cao, L.; Rharbi, Y.; Raez, J.; Winnik, M. A.; Manners, I. *J. Am. Chem. Soc.* **2000**, *122*, 11577–11584.
- Cao, L.; Manners, I.; Winnik, M. A. *Macromolecules* **2002**, *35*, 8258–8260.
- Wang, X.; Guerin, G.; Wang, H.; Wang, Y. S.; Manners, I.; Winnik, M. A. *Science* **2007**, *317*, 644.
- Gädt, T.; Ieong, N. S.; Cambridge, G.; Winnik, M. A.; Manners, I. *Nat. Mater.* **2009**, *8*, 144–150.
- Gilroy, J. B.; Gaedt, T.; Whittell, G. R.; Chabanne, L.; Mitchels, J. M.; Richardson, R. M.; Winnik, M. A.; Manners, I. *Nat. Chem.* **2010**, *2*, 566–570.
- Lazzari, M.; Scalarone, D.; Vazquez-Vazquez, C.; Lopez-Quintela, M. A. *Macromol. Rapid Commun.* **2008**, *29*, 352–357.
- Geng, Y.; Discher, D. E. *J. Am. Chem. Soc.* **2005**, *127*, 12780–12781.
- Petzetakis, N.; Dove, A. P.; O'Reilly, R. K. *Chem. Sci.* **2011**, *2*, 955–960.
- Petzetakis, N.; Robin, M. P.; Patterson, J. P.; Kelley, E. G.; Cotanda, P.; Bomans, P. H. H.; Somerdijk, N. A. J. M.; Dove, A. P.; Epps, T. H., III; O'Reilly, R. K. *ACS Nano* **2013**, *7*, 1120–1128.
- Dyson, M. A.; Sanchez, A. M.; Patterson, J. P.; O'Reilly, R. K.; Sloan, J.; Wilson, N. R. *Soft Matter* **2013**, *9*, 3741–3749.
- Hammer, B. A. G.; Bokel, F. A.; Hayward, R. C.; Emrick, T. *Chem. Mater.* **2011**, *23*, 4250–4256.
- Lee, E.; Hammer, B.; Kim, J. K.; Page, Z.; Emrick, T.; Hayward, R. C. *J. Am. Chem. Soc.* **2011**, *133*, 10390–10393.
- Patra, S. K.; Ahmed, R.; Whittell, G. R.; Lunn, D. J.; Dunphy, E. L.; Winnik, M. A.; Manners, I. *J. Am. Chem. Soc.* **2011**, *133*, 8842–8845.
- Gwyther, J.; Gilroy, J. B.; Rupar, P. A.; Lunn, D. J.; Kynaston, E.; Patra, S. K.; Whittell, G. R.; Winnik, M. A.; Manners, I. *Chem.—Eur. J.* **2013**, *19*, 9186–9197.
- Kamps, A. C.; Fryd, M.; Park, S. J. *ACS Nano* **2012**, *6*, 2844–2852.

- (49) Yin, L.; Hillmyer, M. A. *Macromolecules* **2011**, *44*, 3021–3028.
- (50) Yin, L.; Lodge, T. P.; Hillmyer, M. A. *Macromolecules* **2012**, *45*, 9460–9467.
- (51) Schmelz, J.; Karg, M.; Hellweg, T.; Schmalz, H. *ACS Nano* **2011**, *5*, 9523–9534.
- (52) Schmelz, J.; Schedl, A. E.; Steinlein, C.; Manners, I.; Schmalz, H. *J. Am. Chem. Soc.* **2012**, *134*, 14217–14225.
- (53) Mihut, A. M.; Chiche, A.; Drechsler, M.; Schmalz, H.; Di Cola, E.; Krausch, G.; Ballauff, M. *Soft Matter* **2009**, *5*, 208–213.
- (54) Mihut, A. M.; Drechsler, M.; Möller, M.; Ballauff, M. *Macromol. Rapid Commun.* **2010**, *31*, 449–453.
- (55) Mihut, A. M.; Crassous, J. J.; Schmalz, H.; Ballauff, M. *Colloid Polym. Sci.* **2010**, *288*, 573–578.
- (56) Du, Z. X.; Xu, J. T.; Fan, Z. Q. *Macromol. Rapid Commun.* **2008**, *29*, 467–471.
- (57) Fairley, N.; Hoang, B.; Allen, C. *Biomacromolecules* **2008**, *9*, 2283–2291.
- (58) He, W. N.; Xu, J. T.; Du, B. Y.; Fan, Z. Q.; Wang, X. S. *Macromol. Chem. Phys.* **2010**, *211*, 1909–1916.
- (59) He, W. N.; Zhou, B.; Xu, J. T.; Du, B. Y.; Fan, Z. Q. *Macromolecules* **2012**, *45*, 9768–9778.
- (60) Wang, X.; Liu, K.; Arsenault, A. C.; Rider, D. A.; Ozin, G. A.; Winnik, M. A.; Manners, I. *J. Am. Chem. Soc.* **2007**, *129*, 5630–5639.
- (61) Wang, H.; Wang, X.; Winnik, M. A.; Manners, I. *J. Am. Chem. Soc.* **2008**, *130*, 12921–12930.
- (62) Du, Z. X.; Xu, J. T.; Fan, Z. Q. *Macromolecules* **2007**, *40*, 7633–7637.
- (63) Portinha, D.; Bouteiller, F. B.; Carrot, L. G.; Chassenieux, C.; Pensec, S.; Reiter, G. *Macromolecules* **2007**, *40*, 4037–4042.
- (64) Lazzari, M.; Scalarone, D.; Vazquez-Vazquez, C.; Lopez-Quintela, M. A. *Macromol. Rapid Commun.* **2008**, *29*, 352–357.
- (65) Gädt, T.; Schacher, F. H.; McGrath, N.; Winnik, M. A.; Manners, I. *Macromolecules* **2011**, *44*, 3777–3786.
- (66) Rajagopal, K.; Mahmud, A.; Christian, D. A.; Pajerowski, J. D.; Brown, A. E. X.; Loverde, S. M.; Discher, D. E. *Macromolecules* **2010**, *43*, 9736–9746.
- (67) Schmalz, H.; Schmelz, J.; Drechsler, M.; Yuan, J.; Walther, A.; Schweimer, K.; Mihut, A. M. *Macromolecules* **2008**, *41*, 3235–3242.
- (68) Wang, H.; Winnik, M. A.; Manners, I. *Macromolecules* **2007**, *40*, 3784–3789.
- (69) Wang, H.; Lin, W.; Fritz, K. P.; Scholes, G. D.; Winnik, M. A.; Manners, I. *J. Am. Chem. Soc.* **2007**, *129*, 12924–12925.
- (70) Shen, L.; Wang, H.; Guerin, G.; Wu, C.; Manners, I.; Winnik, M. A. *Macromolecules* **2008**, *41*, 4380–4389.
- (71) He, F.; Gädt, T.; Manners, I.; Winnik, M. A. *J. Am. Chem. Soc.* **2011**, *133*, 9095–9103.
- (72) Mohd Yusoff, S. F.; Hsiao, M.-S.; Schacher, F.; Winnik, M. A.; Manners, I. *Macromolecules* **2012**, *45*, 3883–3891.
- (73) Natalello, A.; Alkan, A.; Friedel, A.; Lieberwirth, A.; Frey, H.; Würm, F. R. *ACS Macro Lett.* **2013**, *2*, 313–316.
- (74) Kloninger, C.; Rehahn, M. *Macromolecules* **2004**, *37*, 1720–1727.
- (75) Keller, A.; Cheng, S. Z. D. *Polymer* **1998**, *39*, 4461–4487.
- (76) Cheng, S. Z. D. *Phase Transitions in Polymers: The Role of Metastable States*; Elsevier: Amsterdam, 2008.
- (77) Qian, J. S.; Lu, Y. J.; Chia, A.; Zhang, M.; Rupar, P. A.; Gunari, N.; Walker, G. C.; Cambridge, G.; He, F.; Guerin, G.; Manners, I.; Winnik, M. A. *ACS Nano* **2013**, *7*, 3754–3766.
- (78) Qian, J. S.; Guerin, G.; Cambridge, G.; Manners, I.; Winnik, M. A. *Macromol. Rapid Commun.* **2010**, *31*, 928–933.
- (79) Brandrup, J.; Immergut, E. H.; Grulke, E. A.; Abe, A.; Bloch, D. T. *Polymer Handbook*; John Wiley & Sons: New York, 2003.
- (80) Gilroy, J. B.; Rupar, P. A.; Whittell, G. R.; Chabanne, L.; Terrill, N. J.; Winnik, M. A.; Manners, I.; Richardson, R. M. *J. Am. Chem. Soc.* **2011**, *133*, 17056–17062.
- (81) For a spot-type SAED profile for randomly oriented cylindrical micelles, see Figure S15.
- (82) Chen, Z.; Foster, M. D.; Zhou, W.; Fong, H.; Reneker, D. H.; Resendes, R.; Manners, I. *Macromolecules* **2001**, *34*, 6156–6158.
- (83) Papkov, V. S.; Gerasimov, M. V.; Dubovik, I. I.; Sharma, S.; Dementiev, V. V.; Pannell, K. H. *Macromolecules* **2000**, *33*, 7107–7115.
- (84) Kulbaba, K.; Manners, I. *Macromol. Rapid Commun.* **2001**, *22*, 711–724.
- (85) Lammertink, R. G. H.; Hempenius, M. A.; Manners, I.; Vancso, G. J. *Macromolecules* **1998**, *31*, 795–800.
- (86) Xu, J. J.; Bellas, V.; Jungnickel, B.; Stuhn, B.; Rehahn, M. *Macromol. Chem. Phys.* **2010**, *211*, 1261–1271.
- (87) Mihut, A. M.; Crassous, J. J.; Schmalz, H.; Drechsler, M.; Ballauff, M. *Soft Matter* **2012**, *8*, 3163–3173.
- (88) See SI for details.
- (89) Rupar, P. A.; Cambridge, G.; Winnik, M. A.; Manners, I. *J. Am. Chem. Soc.* **2011**, *133*, 16947–16957.
- (90) Wunderlich, B. *Macromolecular Physics - Crystal Structure, Morphology, Defects*; Academic Press: New York, 1973.
- (91) Ungar, G.; Putra, E. G. R.; De Silva, D. S. M.; Shcherbina, M. A.; Waddon, A. J. *Adv. Polym. Sci.* **2005**, *180*, 45–87.
- (92) Presa Soto, A.; Gilroy, J. B.; Winnik, M. A.; Manners, I. *Angew. Chem., Int. Ed.* **2010**, *49*, 8220–8223.
- (93) Eloï, J.-C.; Rider, D. A.; Cambridge, G.; Whittell, G. R.; Winnik, M. A.; Manners, I. *J. Am. Chem. Soc.* **2011**, *133*, 8903–8913.